Quantum cutting mechanism in $NaYF_4$:Tb^{3+}, Yb^{3+}

Qianqian Duan,[1] Feng Qin,[1,2] Zhiguo Zhang,[1,2,4] and Wenwu Cao[1,2,3]

[1]*Condensed Matter Science and Technology Institute, Harbin Institute of Technology, Harbin 150001, China*

[2]*Laboratory of Sono- and Photo-Theranostic Technologies, Harbin Institute of Technology, Harbin 150001, China*

[3]*Materials Research Institute, The Pennsylvania State University, Pennsylvania 16802, USA*

[4]*e-mail: zhangzhiguo@hit.edu.cn*

[5]*e-mail: dzk@psu.edu*

Received November 21, 2011; revised December 15, 2011; accepted December 16, 2011; posted December 16, 2011 (Doc. ID 158585); published February 8, 2012

A quantum cutting mechanism for the sublinear near-IR power dependence property in Tb^{3+}–Yb^{3+} codoped $NaYF_4$ powders were investigated both experimentally and theoretically. The slopes of Yb^{3+} luminescence intensity versus excitation power were fitted to be between 0.5 and 1. We have developed a quantum cutting rate equation model to explain the anomalous sublinear phenomenon and an assessment factor was introduced to help understand the physical mechanism. Experimental results showed that the linear downconversion process combined with second-order nonlinear process induced the sublinear power dependence property with the latter to be the dominant process.

OCIS codes: 160.2540, 160.2750, 160.4760.

Near-IR quantum cutting using Re^{3+}–Yb^{3+} pairs could convert one UV/visible photon ($\lambda < 550$ nm) to two near-IR photons ($\lambda \sim 1000$ nm), which are just above the bandgap of crystalline silicon (Si). Therefore, quantum cutting could be a promising option to reduce the thermal losses and enhance the efficiency of Si solar cells [1–5]. Near-IR quantum cutting using Tb^{3+}–Yb^{3+} codoping was first reported in a $Yb_xY_{1-x}PO_4$:Tb^{3+} powder sample [6], where the luminescence decay curves of Tb^{3+} were analyzed by Monte Carlo simulation method and the cooperative quantum cutting mechanism was demonstrated, as illustrated by the solid lines in Fig. 1. Since then, quantum cutting based on Tb^{3+}–Yb^{3+} codoping has been reported in many other host materials [5], and the cooperative quantum cutting mechanism is generally accepted.

So far, there have been few theoretical studies on the quantum cutting mechanism for the Tb^{3+}–Yb^{3+} couple. However, the underlying energy transfer mechanism of the quantum cutting process is still not quite clear, and there is a dispute in the cooperative quantum cutting energy transfer process from Tb^{3+} to Yb^{3+} [4]. Some researchers have argued that the downconversion emission intensities would increase linearly versus the excitation intensity [1–3], while others believed that a nonlinear second-order downconversion process is responsible for the cooperative quantum cutting, i.e., the slopes of the power dependence curves of Yb^{3+} luminescence should be 0.5 instead of 1 [7–8]. According to the above reports, the near-IR quantum cutting may be either a linear or a second-order process in a variant host environment, which indicates a different energy transfer nature responsible for the quantum cutting process between Tb^{3+} and Yb^{3+}. A further detailed in-depth understanding of the quantum cutting mechanism would be beneficial for proper choice of doping ions to further improve the quantum efficiency [5].

We have performed numerous studies on the near-IR quantum cutting mechanism. A series of samples, including oxyfluoride glass, oxide powders, oxide ceramics, and fluoride powders, were prepared by different methods, such as the high-temperature solid-state reaction method, the solgel method, and the coprecipitation method. A maximum quantum efficiency of 148% was achieved before the concentration quenching of Yb^{3+} in our samples by analyzing the measured lifetime values. It was found experimentally that the slopes of Yb^{3+} luminescence power dependence curves were fitted to be 1 in oxyfluoride glass, oxide powders, and oxide ceramics samples, and 0.6–0.8 in fluoride powder samples. We have proposed a rate equation model to describe the linear process [9].The near-IR quantum cutting process in fluoride powder samples is neither a linear process with a slope of 1 nor a second-order nonlinear downconversion process with a slope of 0.5, and the previous linear [9] and second-order nonlinear [7] downconversion rate equation models cannot interpret this anomalous sublinear process. In this Letter, the quantum cutting mechanism of near-IR luminescence in $NaYF_4$ was investigated. The luminescence spectra and power dependence curves were measured. We proposed that the linear and second-order downconversion processes played a coreaction role in this sublinear process. The corresponding rate equation model was set up to describe the energy transfer process and explore the quantum cutting mechanism of Tb^{3+}–Yb^{3+} codoping situation.

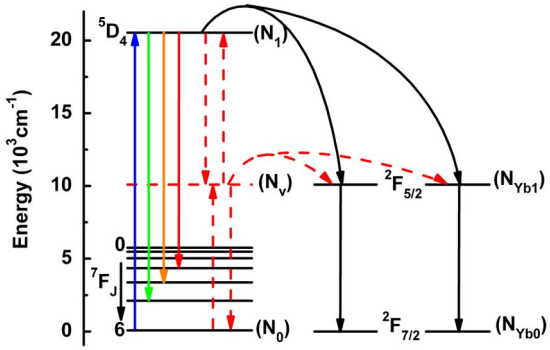

Fig. 1. (Color online) Schematic energy level diagram in a Tb^{3+}–Yb^{3+} codoped host showing the energy transfer mechanism of the near-IR quantum cutting under the excitation of the $^7F_6 \rightarrow {}^5D_4$ (Tb^{3+}) transition.

$NaYF_4$ powder samples codoped with 1 mol % Tb^{3+}–x mol% Yb^{3+} ions ($x = 0$, 5, 10) were synthesized by the coprecipitation method [10]. Figure 2 depicts the emission spectra of $NaYF_4$ codoped with Tb^{3+} and Yb^{3+} ions under the excitation of the $^7F_6 \rightarrow {}^5D_4$ (Tb^{3+}) transition by a 473 nm continuous wave laser. As shown in Fig. 2, the emission bands centered at 543, 585, and 622 nm in the visible range could be assigned to the transitions of $^5D_4 \rightarrow {}^7F_J$ ($J = 5, 4, 3$, respectively). The broad near-IR emission band around 1 μm ascribed to the transition of $^2F_{5/2} \rightarrow {}^2F_{7/2}$ (Yb^{3+}) was observed under the excitation of a 473 nm laser when Yb^{3+} was introduced. Since the 473 nm photons were far from the resonant excitation for Yb^{3+}, the appearance of near-IR emission implied an energy transfer process from Tb^{3+} to Yb^{3+}. Moreover, the emission intensity of Tb^{3+} decreased with the introduction of Yb^{3+} due to another energy transfer path produced by Yb^{3+}, which was further indicative of energy transfer from Tb^{3+} to Yb^{3+}.

To get more information about the quantum cutting luminescence, the power dependence curves for the luminescence of $^5D_4 \rightarrow {}^7F_J$ (Tb^{3+}) and $^2F_{5/2} \rightarrow {}^2F_{7/2}$ (Yb^{3+}) were measured and plotted in a double logarithmic scale (shown in Fig. 3). The intensities of Tb^{3+} luminescence exhibited linear dependence on the excitation power. However, the power dependence property for the luminescence of Yb^{3+} was anomalous. The slopes of Yb^{3+} luminescence intensity versus excitation power were fitted to be 0.7–0.8, and the slopes were a little different when the concentration of Yb^{3+} was changed.

To get a deeper comprehension of the energy transfer mechanism in $NaYF_4$, the power dependence behavior was theoretically investigated based on rate equations. According to our previous report, $N_{Yb1} \propto \rho$, $N_1 \propto \rho$, and both slopes of Tb^{3+} and Yb^{3+} luminescence intensities versus the excitation power are 1, which is consistent with the expected linear process of downconversion [9]. However, this theoretical model could not interpret the sublinear power dependence curves of Yb^{3+} in $NaYF_4$. This indicated another downconversion process in $NaYF_4$, which induced the sublinear power dependence.

Considering that the near-IR luminescence power dependence curve of the second-order quantum cutting process has a slope of 0.5, it is reasonable to assume that both the linear and second-order near-IR quantum cutting processes existed simultaneously in Tb^{3+}–Yb^{3+} codoped $NaYF_4$. Based on the linear cooperative quantum cutting model, we propose here a new rate equation model to depict the sublinear quantum cutting mechanism in Tb^{3+}–Yb^{3+} coupled pair.

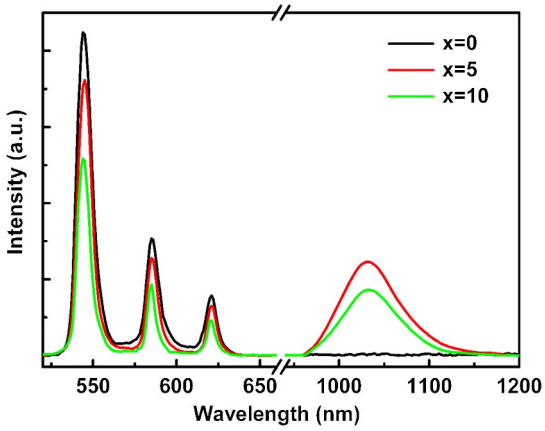

Fig. 2. (Color online) Emission spectra of Tb^{3+}–Yb^{3+} codoped $NaYF_4$ powder samples under a 473 nm cw laser excitation.

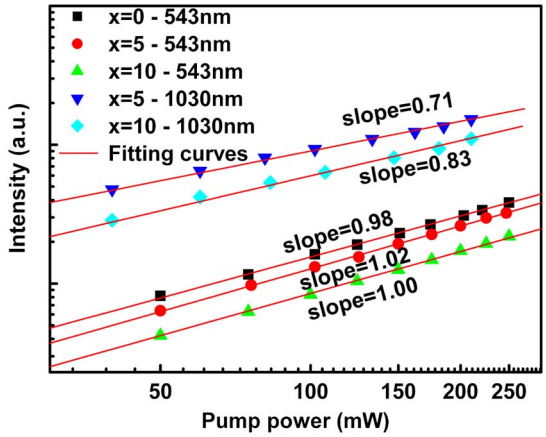

Fig. 3. (Color online) Double logarithmic plot of Tb^{3+} and Yb^{3+} emission intensities versus the pump power of the 473 nm laser for Tb^{3+}–Yb^{3+} codoped $NaYF_4$ powder samples.

Energy transfer could occur with the participation of virtual and intermediate metastable states when investigating a multiple-photon cooperative sensitization luminescence process [11]. This concept has been frequently used to analyze and interpret the cooperative sensitization upconversion mechanism in Tb^{3+}–Yb^{3+} coupled ions [12–13]. The cooperative quantum cutting could be considered as the opposite process of the cooperative sensitization upconversion process in Tb^{3+}–Yb^{3+} codoped materials, and the virtual state was used to depict the downconversion mechanism by Strek *et al.* [7], hence we assume that a virtual energy level of Tb^{3+} could participate in the quantum cutting process. This virtual energy level is located at the middle position (around 10,000 cm^{-1}) between the ground state and the $^5D_4$ energy level of Tb^{3+}, which matches well with the energy level of Yb^{3+} (shown in Fig. 1 with dotted line).

We consider the case with the population of the virtual energy level being a constant in a very short time and the Tb^{3+}–Yb^{3+} ion couple can realize energy transfer through this virtual energy level. Let us first consider the population and depopulation processes of Tb^{3+} without the effect of Yb^{3+}. The population process of the virtual state was through a cross-relaxation process with the corresponding parameter D_1. During the population process, another cross-relaxation process with the corresponding parameter D_2 also occurred as a depopulation process at the same time. Considering Tb^{3+} separately, the rate equations may be written as

$$\frac{dN_1}{dt} = \sigma\rho N_0 - A_1 N_1 + D_2 N_v^2 - D_1 N_1 N_0, \qquad (1)$$

$$\frac{dN_v}{dt} = 2D_1 N_1 N_0 - 2D_2 N_v^2, \qquad (2)$$

where N_0, N_1, N_v, N_{Yb0}, and N_{Yb1} are the energy level populations of the $^7F_6$ (Tb^{3+}), $^5D_4$ (Tb^{3+}), virtual level (Tb^{3+}), $^2F_{7/2}$ (Yb^{3+}), and $^2F_{5/2}$ (Yb^{3+}), respectively; σ

is the absorption cross section from the ground state of Tb^{3+}; ρ is the pump constant; and A_1 and A_2 are the radiation rates of $^5D_4$ (Tb^{3+}) and $^2F_{5/2}$ (Yb^{3+}) levels, respectively. According to the steady-state solution, the populations of these levels have the following relations with the pump constant:

$$N_1 = \frac{\sigma\rho N_0}{A_1} \propto \rho, \tag{3}$$

$$N_v = \left(\frac{D_1 N_1 N_0}{D_2}\right)^{1/2} \propto \rho^{1/2}. \tag{4}$$

Considering the interactions in the Tb^{3+}–Yb^{3+} coupled pair system, neglecting the energy transfer from Yb^{3+} to Tb^{3+} and the upconversion process of Tb^{3+}, the rate equations become

$$\frac{dN_1}{dt} = \sigma\rho N_0 - A_1 N_1 - D_1 N_1 N_0 - wN_1 N_{\mathrm{Yb0}}^2, \tag{5}$$

$$\frac{dN_{\mathrm{Yb1}}}{dt} = 2w' N_v N_{\mathrm{Yb0}} + 2wN_1 N_{\mathrm{Yb0}}^2 - A_2 N_{\mathrm{Yb1}}, \tag{6}$$

where w is the corresponding parameter for the cooperative energy transfer process from $^5D_4$ (Tb^{3+}) to Yb^{3+}, and w' is the energy transfer rate constant associated with energy transfer from the virtual state of Tb^{3+} to Yb^{3+}. The steady-state solutions are

$$N_1 = \frac{\sigma\rho N_0}{A_1 + wN_{\mathrm{Yb0}}^2 + D_1 N_0} \propto \rho, \tag{7}$$

$$N_{\mathrm{Yb1}} = \frac{2w' N_{\mathrm{Yb0}}}{A_2} N_v + \frac{2wN_{\mathrm{Yb0}}^2}{A_2} N_1. \tag{8}$$

It is clear that the luminescence intensity of Tb^{3+} increases linearly with the pump power. To analyze the power dependence of Yb^{3+}, we considered two extreme cases. If the energy transfer from the virtual state of Tb^{3+} is the dominant population process of Yb^{3+}, the second term on the right-hand side (RHS) of Eq. (6) could be neglected, so that

$$N_{\mathrm{Yb1}} = \frac{2w' N_{\mathrm{Yb0}}}{A_2} N_v \propto \rho^{1/2}, \tag{9}$$

which corresponds to the second-order nonlinear process with a slope of 0.5. In contrast, if the energy transfer from the $^5D_4$ energy level of Tb^{3+} is the dominant population process of Yb^{3+}, the first term on the RHS of Eq. (6) becomes negligible, so that

$$N_{\mathrm{Yb1}} = \frac{2wN_{\mathrm{Yb0}}^2}{A_2} N_1 \propto \rho, \tag{10}$$

which corresponds to the linear process with a slope of 1.

The slopes of near-IR luminescence power dependence curves in $NaYF_4$ are between 0.5 and 1, which is between the two limiting cases. Therefore, it is reasonable to believe that the nonlinear second-order process combined with the linear process induced the sublinear power dependence. From Eqs. (8)–(10), we proposed the simple expression below to weigh the proportions of the two mechanisms:

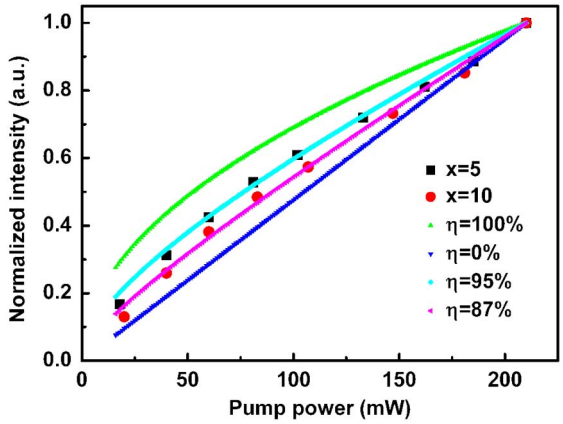

Fig. 4. (Color online) Experimental and simulated power dependence curves of Yb^{3+} luminescence for Tb^{3+}–Yb^{3+} codoped $NaYF_4$ powder samples.

$$I_{\mathrm{Yb}} \propto N_{\mathrm{Yb1}} = \chi[\eta\rho^{1/2} + (1-\eta)\rho], \tag{11}$$

where χ is the normalization coefficient and η is the proportion of the second-order nonlinear process in the quantum cutting process, which is used as an assessment factor to evaluate the weight of the nonlinear process. Both coefficients in Eq. (11) could be determined by Eq. (8). Fitting the experimental power dependence curves of Yb^{3+} using Eq. (11), the calculated results were in accordance with the experimental curves, which verified the validity of our rate equation model. The optimum values of η were fitted to be 95% and 87% for 5% and 10% Yb^{3+} concentrations, respectively (shown in Fig. 4). Therefore, the nonlinear quantum cutting process was theoretically estimated to be the dominant mechanism in Tb^{3+}–Yb^{3+} codoped $NaYF_4$.

References

1. B. S. Richards, Sol. Energy Mater. Sol. Cells **90**, 2329 (2006).
2. T. Trupke, M. A. Green, and P. Wurfel, J. Appl. Phys. **92**, 1668 (2002).
3. B. M. van der Ende, L. Aarts, and A. Meijerink, Phys. Chem. Chem. Phys. **11**, 11081 (2009).
4. B. S. Richards, Sol. Energy Mater. Sol. Cells **90**, 1189 (2006).
5. Q. Y. Zhang and X. Y. Huang, Prog. Mater. Sci. **55**, 353 (2010).
6. P. Vergeer, T. J. H. Vlugt, M. H. F. Kox, M. I. den Hertog, J. P. J. M. van der Eerden, and A. Meijerink, Phys. Rev. B **71**, 014119 (2005).
7. W. Strek, A. Bednarkiewicz, and P. J. Dereń, J. Lumin. **92**, 229 (2001).
8. D. Q. Chen, Y. L. Yu, Y. S. Wang, P. Huang, and F. Y. Weng, J. Phys. Chem. C **113**, 6406 (2009).
9. Q. Q. Duan, F. Qin, D. Wang, W. Xu, J. M. Cheng, Z. G. Zhang, and W. W. Cao, J. Appl. Phys. **110**, 113503 (2011).
10. G. S. Yi, H. C. Lu, S. Y. Zhao, Y. Ge, W. J. Yang, D. P. Chen, and L. H. Guo, Nano Lett. **4**, 2191 (2004).
11. P. P. Feofilov and V. V. Ovsyankin, Appl. Opt. **6**, 1828 (1967).
12. G. M. Sally, R. Valliente, and H. U. Guedel, J. Lumin. **94**, 305 (2001).
13. I. Hernández, N. Pathumakanthar, P. B. Wyatt, and W. P. Gillin, Adv. Mater. **22**, 5356 (2010).